Exciton-Polariton Topological Insulator with an Array of Magnetic Dots

M. Sun,[1,2] D. Ko,[1,2] D. Leykam,[1,2] V. M. Kovalev,[3,4] and I. G. Savenko[1,2,*]

[1] *Center for Theoretical Physics of Complex Systems, Institute for Basic Science (IBS), Daejeon 34126, Republic of Korea*

[2] *Basic Science Program, Korea University of Science and Technology (UST), Daejeon 34113, Republic of Korea*

[3] *A. V. Rzhanov Institute of Semiconductor Physics, Siberian Branch of Russian Academy of Sciences, Novosibirsk 630090, Russia*

[4] *Department of Applied and Theoretical Physics, Novosibirsk State Technical University, Novosibirsk 630073, Russia*

(Received 25 July 2019; revised manuscript received 1 November 2019; published 11 December 2019)

Recently, there have been several proposals on exciton-polariton topological insulators, most of which have required strong external magnetic fields induced by bulky superconducting coils. We propose an alternative design for a polariton topological insulator, where excitons are in the proximity of an additional layer of a ferromagnetic material, with a predefined magnetic moment located between the pillars of the cavity. Our design supports a variety of topological phases and transitions between Chern numbers ± 2 and ± 1 by varying either the magnetic moment of the ferromagnetic material or the spin-orbit coupling between different spin projections, thus enabling compact polariton devices harnessing switchable topological edge modes.

DOI: 10.1103/PhysRevApplied.12.064028

I. INTRODUCTION

Robust transport of particles in topologically nontrivial systems occurs due to the existence of protected edge modes at interfaces between media with different topological properties [1–3]. Such edge states are robust against disorder, which makes them appealing from fundamental and application-oriented viewpoints. Phase transitions to topological insulating phases were originally discovered in the context of the integer quantum Hall effect [4], where a nonzero quantized Chern number is associated with disorder-robust quantization of the particle current (and conductivity) in strong external magnetic fields. Later, this idea was extended to the anomalous quantum Hall and quantum spin Hall effects [5–8], where an external net magnetic field is not required—instead, it is replaced by other effects such as time-reversal symmetry breaking induced by internal magnetization of the material [9,10] or strong spin-orbit coupling. Topological phases have now been extended to various physical systems, including photonics, cold atoms, and acoustics [11–13].

A recent experiment has demonstrated an exciton-polariton topological Chern insulator [14]. Distinct from other platforms, the nontrivial topological phase arose from a combination of *three* main ingredients: an artificial lattice made of micrometer-sized pillars, excitonic spin-orbit coupling or photonic TE-TM splitting, and an external magnetic field in the Faraday configuration [15,16]. The lattice creates a finite Brillouin zone with energy bands in reciprocal space, the spin-orbit coupling creates a momentum-dependent energy splitting between spin states without opening a band gap, and the external magnetic field induces a Zeeman splitting between spin-up and spin-down exciton-polaritons. Notably, all three effects are required to create a topological band gap in which the protected edge states reside, in contrast to other platforms, where a lattice combined with a uniform or staggered magnetic field is sufficient.

So far, theoretical and experimental studies on the exciton-polariton topological insulators have focused on the case of a uniform external magnetic field [15–19]. In order to observe a measurable band gap, a large external magnetic field (up to 5 T) has been used, requiring superconducting coils and cryogenic temperatures [14]. Evidently, this strong external magnetic field is a significant drawback limiting potential applications in real devices, such as using the edge states for the disorder-robust transfer of optical signals and information processing. In particular, essential advantages of microcavity samples such as their compactness and potential for room-temperature operation are compromised or even negated. It is therefore crucial to explore application-friendly mechanisms and techniques by which topological polaritons can be created without an external magnetic field.

*savenko.j@mail.ru

The existing proposals have been based on effects such as nonlinear dynamics under resonant pumping [20], time- or spin-dependent pumping [21], and spontaneous symmetry breaking [22–24]. However, all these proposals have their technological limitations. For example, the use of the nonlinear terms due to particle interaction requires strong resonant pumping of the sample in order to excite the edge as a perturbation [15,19]; and spin-dependent pumping demands independent treatment of each lattice site, which makes the design of even a single experiment tricky, not to say that it makes the creation of nontrivial topology-based logic impossible.

In this paper, we propose an easily realizable alternative design for an exciton-polariton topological insulator in which the external uniform magnetic field is replaced by an internal inhomogeneous magnetization, produced by a magnetic material (MM) embedded within the microcavity [25,26]. We show that the resulting staggered magnetic field is capable of opening a topological band gap and can yield topological transitions between different Chern numbers (± 2 to ∓ 1) as either the magnetic field or spin-orbit coupling strength is varied, similar to the uniform external field case [27]. With our approach, superconducting coils and other bulky equipment can be eliminated, which is a step toward translating exciton-polariton topological insulators into actual devices.

II. SYSTEM SCHEMATIC

Let us consider polaritons loaded in the honeycomb lattice shown in Fig. 1(a). In recent experiments [14], an external homogeneous magnetic field perpendicular to the lattice has been applied to break time-reversal symmetry. To get rid of the setup required to generate a sufficiently strong magnetic field, we use a layer of magnetic material (MM), which represents an array of submicron magnetic quantum dots. When magnetized, they can replace an external field. Let us first consider the case in which the MM is located on the pillars from the top, thus covering the upper DBR. The MM then represents an array of magnetic quantum dots (QDs) [see Fig. 1(b)].

The magnetic field from a single disk-shaped quantum dot of radius R reads as follows [28,29]:

$$B_z(r,z) = 2\pi\mu_0 MR\int_0^\infty J_0(rq)J_1(Rq)e^{-|z|q}q\,dq, \qquad (1)$$

where $\mu_0 = 4\pi \times 10^{-7}$ H/m is the vacuum permeability, $M = 8\times 10^4$ Oe m is the two-dimensional magnetization perpendicular to the disk-shaped quantum dot, the J_i are the Bessel functions, r is the distance from the center of the QD, q is the in-plane momentum (to be integrated out), and z is the vertical distance from the MM to the QW.

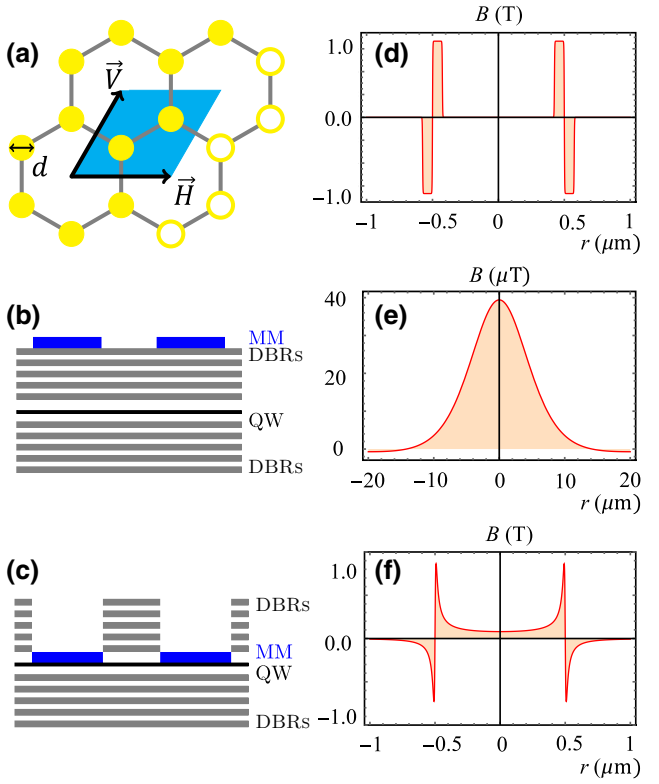

FIG. 1. Left panels: the system schematic. (a) A honeycomb lattice made of pillars of the etched cavity; the yellow empty rings denote the edge region. The direction of the edge is along the $\vec{V}$ direction. (b) The setup using MM placed at the top of the distributed Bragg reflector (DBR). (c) The setup using MM placed at the top of the quantum well (QW) (close to the exciton layers). Right panels: the magnetic field profile in the case of a single MM disk with radius $R = 0.5$ μm. (d) The magnetic field used in the numerical calculations: rectangle functions of width dw. (e) The magnetic field for case (b) and 10 μm away from the QW. (f) The magnetic field for case (c) and 8 nm away from the QW.

The integral in Eq. (1) can be calculated semianalytically, using the special functions [30], giving

$$B_z = \frac{\left[f^2(R^2 - r^2 - z^2)E(f) + (1-f^2)4rRK(f)\right]}{4\mu_0^{-1}M^{-1}(Rr)^{3/2}(1-f^2)f^{-1}}, \qquad (2)$$

where $f = \sqrt{4rR/[z^2 + (r+R)^2]}$ and $K(f)$ and $E(f)$ are the elliptic integrals of the first and second kind, respectively.

Figure 1(e) shows the calculated profile of the z projection of the magnetic field. Since the distance between the layers of the excitons and the MM amounts to $z \sim 10$ μm in this case (according to a typical size of a microcavity), the resulting effective magnetic field acting on the excitons is only of the order of μT, which is too small to create a useful topological band gap. This is because B_z in Eq. (2) decays exponentially with z.

To achieve a strong enough magnetic field, one has to reduce the separation between the MM and the QW. Thus we consider the scheme shown in Fig. 1(c), where the microcavity is etched to form a honeycomb lattice and a layer of MM is deposited in the etched regions. This allows the MM to be placed very close to the QWs, where the excitons reside, leading to interlayer separations of only $z \sim 1-20$ nm and strong magnetic fields (approximately 1 T). In this case, the magnetic field profile [Fig. 1(f)] has a very different shape: it is strongly localized at the micropillar-MM boundary, where it also changes sign. Thus, the magnetic field is *staggered* with zero net flux. In Fig. 1(f), we show that a MM with the shape of a disk with radius $R = 0.5$ μm produces a magnetic field of approximately 1 T at a distance of 8 nm.

To prepare the cavity with embedded magnetic quantum dots, one should first grow the cavity (multilayered structure); second, one should etch micropillars to form the desired lattice potential; and, third, one should deposit the magnetic material onto the whole structure from the top. In this way, part of the magnetic material will be on the edges of the pillars. However, as our calculations explicitly demonstrate, such remote magnetic field sources will not make a substantial contribution and can be disregarded. Finally, by heating the sample above the Curie temperature and exposing it to a strong magnetic field, we can magnetize the sample and make it a permanent magnet.

III. TRANSPORT OF EXCITON-POLARITONS

To determine whether this kind of staggered magnetic field configuration is capable of inducing topological edge states, we compute the band structure and Chern numbers of the polariton honeycomb lattice numerically. Due to the computational limitations (finite discretization), we neglect the weak magnetic field inside and far away from the micropillars and we approximate B_z with a step-function profile of width dw, shown in Fig. 1(d). We describe the time evolution of the exciton-polaritons in the cavity by means of the Gross-Pitaevskii equation,

$$i\hbar\frac{\partial\psi_\pm}{\partial t} = -\frac{\hbar^2}{2m_{\text{eff}}}\nabla^2\psi_\pm + V\psi_\pm + \Delta_\pm^{\text{eff}}\psi_\pm + \beta^{\text{eff}}\left(\partial_x \mp i\partial_y\right)^2\psi_\mp, \tag{3}$$

where $\psi_\pm$ are the wave functions of polaritons with up- and down-polarization; m_{eff} is the effective mass; the first term on the right-hand side denotes the free-particle propagation, V is the potential of the honeycomb lattice with lattice constant 3 μm and site diameter $d = 0.75$ μm; and $\Delta_\pm^{\text{eff}}$ is the effective Zeeman splitting due to the presence of the MM with the shape presented in Fig. 1(d). In the calculations, we assume the lateral size of the MM to be the same as the well of honeycomb lattice and the width of the rectangle functions [Fig. 1(d)] $dw = 0.15$ μm; β^{eff} is an effective TE-TM splitting. We choose the Hopfield coefficients to be $|X_H|^2 = 1 - |C_H|^2 = 0.3$. This gives us the effective polariton mass $m_{\text{eff}} \approx m_C/|C_H|^2$, with the effective mass of the cavity photon $m_C = 3.23 \cdot 10^{-5} m_e$, where m_e is the free-electron mass. For polaritons, we have a similar (to excitons) definition of the effective Zeemann splitting and the TE-TM splitting, $\Delta_\pm^{\text{eff}} = |X_H|^2\Delta_\pm$ and $\beta^{\text{eff}} = \beta|C_H|^2$. In order to quantitatively estimate the magnetic field, we use the Zeeman splitting determined by the relation $\Delta_+ - \Delta_- = g_x\mu_B|\mathbf{B}|$, where $g_x\mu_B \approx 180$ μeV T^{-1} for excitons [31]. Thus, for a Zeeman-splitting term equal $\Delta = |\Delta_\pm| = 1$ meV, the peak magnetic strength is approximately equal to 5.5 T, which means the distance of the MM away from the QW is 1 nm.

IV. PHASE DIAGRAM AND EDGE MODES

First, we compute the bulk bands of Eq. (3) by assuming a periodic structure and the Bloch-wave *Ansatz* $\psi_\pm = u_\pm(\mathbf{k},\mathbf{r})e^{i\mathbf{k}\cdot\mathbf{r}+iEt}$. Second, we find the bulk Bloch-wave eigenstates and the Chern number [32]:

$$C = \sum_{E_n<E_g} C_n = \frac{1}{2\pi i}\sum_{E_n<E_g}\oint_{\text{BZ}} F_{\mu\nu}^n d^2k, \tag{4}$$

with BZ representing the Brillouin zone, where the Berry connection $A_n(k)$ $(n = 1, 2)$ in the nth band below the energy gap $(E_n < E_g)$ and the associated field strength $F_{\mu\nu}(k)$ are defined as follows:

$$A_\mu = \langle n(k)|\partial_\mu|n(k)\rangle,$$
$$F_{\mu\nu}(k) = \partial_\mu A_\nu(k) - \partial_\nu A_\mu(k), \tag{5}$$

where $|n(k)\rangle$ is the eigenvector of the nth Bloch band and the inner product denotes integration over the unit cell. The unit vectors μ and ν denote the directions of the two reciprocal-lattice vectors.

By solving Eq. (4) for the system described by Eq. (3), we can plot the Chern number [Fig. 2(a)], using the following parameters: $\Delta_\pm = [0.3 \sim 1.0]$ meV and the TE-TM splitting is $\beta = [0.1 \sim 0.3]$ meV μm^2. As shown in Fig. 2(a), the system can possess different Chern numbers, depending on the parameters. The phase transition between Chern numbers $C = 2$ and $C = -1$ is due to the closing of the gap at the M point and then opening it again. Similar behavior has been reported in Ref. [27] for the case of a homogeneous external magnetic field.

To verify the existence of topological edge states, we also compute the energy spectrum of a semi-infinite structure (with 20 unit cells in the $\vec{H}$ direction and twisted boundary conditions in the $\vec{V}$ direction). Typical spectra for the two topological phases are plotted in Figs. 2(b) and 2(c), revealing both the bulk bands and band gaps hosting one- and two-edge states, respectively, in the gap between the second and third bands.

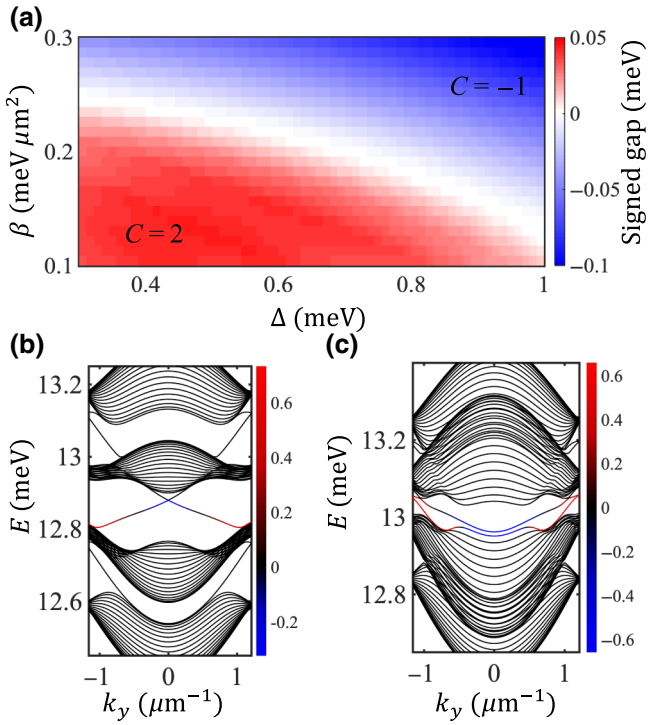

FIG. 2. (a) The phase diagram for the Chern numbers with the TE-TM splitting $0.1 \backsim 0.3$ meV μm^2 and Zeeman splitting $0.3 \backsim 1.0$ meV. The color bar indicates the size of the direct gap multiplied by the sign of the Chern number in the units of [meV]. (b),(c) Spectra of semi-infinite systems with Chern numbers $C = -1$ and $C = 2$, respectively. The color indicates the polarization imbalance, $I = (|\psi_+|^2 - |\psi_-|^2)/(|\psi_+|^2 + |\psi_-|^2)$. For $C = -1$ case, the edge mode is calculated at $\Delta = 0.95$ meV and $\beta = 0.27$ meV μm^2. For $C = 2$ case, the edge mode is calculated at $\Delta = 0.46$ meV and $\beta = 0.13$ meV μm^2.

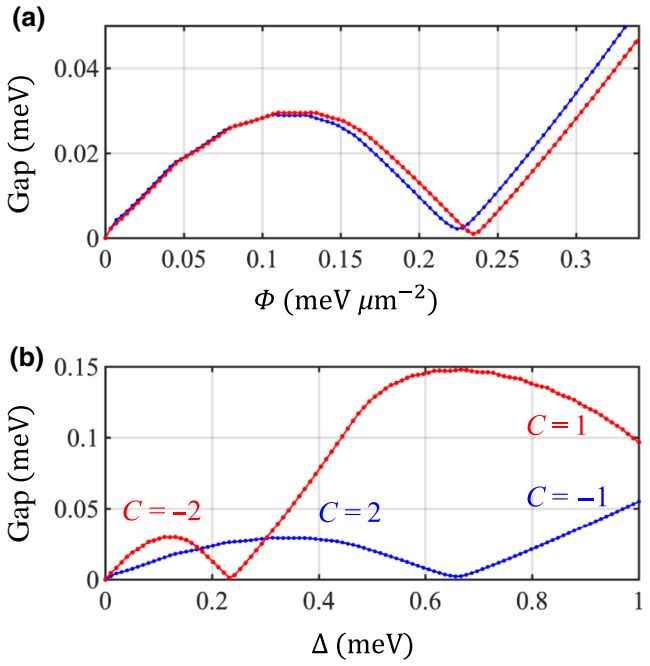

FIG. 3. (a) The band gap as a function of the absolute flux. (b) The band gap as a function of the peak value of the Zeeman splitting. The blue lines show the magnetic dot case and the red lines a homogeneous magnetic field. The TE-TM splitting is fixed to $\beta = 0.2$ meV μm^2.

V. COMPARISON WITH THE HOMOGENEOUS CASE

An important difference between the MM and the external magnetic field cases is the magnitude of the magnetic flux. In the MM case, the total net flux within one unit cell is almost zero due to strong localization of the magnetic field. To compare the MM and the external magnetic field cases, we define the absolute value of the flux on the plane by the integral over a single unit cell region as the unit:

$$\Phi = \frac{\oint_S |\Delta_\pm|\, ds}{S}, \tag{6}$$

where S is the area of the unit cell. Since the Zeeman splitting is proportional to the magnetic field, we can compare the band gaps (between the second and third levels) as functions of the absolute flux in the homogeneous and MM cases. In what follows, we assume that the direction of the magnetic field is the same as the direction of the outer edge of the MM. Figure 3(a) shows that given the same value of the absolute magnetic flux, the gap closes and reopens similarly.

We can also compare the magnitude of the gap as a function of the peak value of the magnetic field, i.e., the peak intensity of the Zeeman splitting. Figure 3(b) demonstrates the sizes of the gaps in the MM and homogeneous cases as functions of the peak value of the Zeeman splitting. We also label the Chern numbers of both cases before and after the gap is closed. Obviously, in the homogeneous case, the gap closes much earlier than in the MM case.

VI. CAVITY WITH A MM EXPOSED TO AN EXTERNAL MAGNETIC FIELD

Having a cavity with embedded MM, one can in addition apply a homogeneous magnetic field to the sample. The resulting field represents a superposition of two magnetic field profiles (Fig. 4).

Let us first consider the case in which the external magnetic field $\mathbf{B}_{\rm ex}$ is parallel to the outside edge of the MM, $\mathbf{B}_{\rm MM}$, as shown in the inset of Fig. 4(a). In this situation, we see further additional phase transitions in the red and green curves. Specifically, we can classify two distinct regimes. The first is when the MM is weak ($\Delta < 0.2$ meV). With the increasing homogeneous magnetic field ($\Delta_{\rm ex}$, from green to red curve), the system undergoes a phase transition from Chern number $C = -2$ to $C = 1$; Second, when the MM is

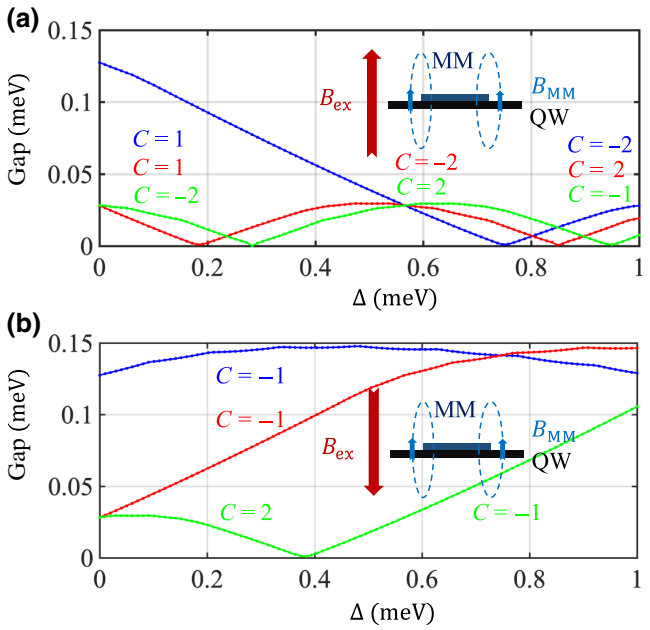

FIG. 4. The mutual effect of MM and an external magnetic field. The x axis labels the intensity of the local magnetic field of the MM. The different colors reflect the different magnitudes of the external magnetic field, $B_{ex} \approx 2.8$, 1.7, and 0.5 T, corresponding to the Zeeman splittings $\Delta_{ex} = 0.5$ (blue), 0.3 (red), and 0.1 meV (green). The Chern numbers are labeled before and after each gap. The TE-TM splitting is fixed at $\beta = 0.2$ meV μm^2.

moderately strong (0.3 meV $< \Delta <$ 0.8 meV), the Chern number changes from $C = 2$ to $C = -2$ as Δ_{ex} increases.

Figure 4(b) shows the effect of the oppositely directed external magnetic field. The red and blue curves show that we can efficiently enlarge the size of the gap in the $C = -1$ case. The size of the gap is vital in topological polaritonic systems, since the finite lifetime of the exciton-polaritons can broaden the bandwidth of the spectrum and diminish and destroy nontrivial topological properties. We also conclude that the combination of two magnetic fields reduces the strength of the external magnetic field required to generate a topological insulator state with a given band gap.

VII. DISCUSSION AND CONCLUSIONS

We show that a local magnetic field due to the presence of a magnetic material can be sufficiently strong to open a gap at the Dirac point and allow for the observation of nontrivial topological states in an exciton-polariton system loaded in a honeycomb lattice. With the change of the intensity of the built-in magnetic field or the TE-TM splitting, the system undergoes a phase transition between two nontrivial states with the Chern numbers ± 2 and ∓ 1.

The key advantage of this setup is the size of the system, which can be much smaller than the one requiring a homogeneous external magnetic field. This can be highly beneficial for future experiments and applications in devices. Furthermore, we study the Chern numbers and gap sizes as functions of the magnetic flux strength and the peak value of the magnetic field. The results show that the design with the use of magnetic material and the regular homogeneous case demonstrate similar behavior.

Furthermore, we explore the joint effect of the internal magnetic material field with an external magnetic field. Depending on the relative direction of the two fields, one can switch between the Chern numbers. This switching can be performed "on the fly," since it is only dependent on a small change of the external magnetic field, thereby enabling control over the number and/or direction of the topological edge states. By reversing the direction of the external magnetic field, one can also keep the Chern number the same but enlarge the size of the gap significantly, thus increasing the speed of the edge state. This allows us to propagate polaritons over greater distances before they decay due to their finite lifetime.

ACKNOWLEDGMENTS

We thank Professor D. Solnyshkov for useful discussions. This work was supported by the Institute for Basic Science in Korea (Projects No. IBS-R024-D1 and No. IBS-R024-Y1).

[1] M. Z. Hasan and C. L. Kane, Colloquium: Topological insulators, Rev. Mod. Phys. **82**, 3045 (2010).
[2] X.-L. Qi and S.-C. Zhang, Topological insulators and superconductors, Rev. Mod. Phys. **83**, 1057 (2011).
[3] C.-K. Chiu, J. C. Y. Teo, A. P. Schnyder, and S. Ryu, Classification of topological quantum matter with symmetries, Rev. Mod. Phys. **88**, 035005 (2016).
[4] K. V. Klitzing, G. Dorda, and M. Pepper, New Method for High-Accuracy Determination of the Fine-Structure Constant Based on Quantized Hall Resistance, Phys. Rev. Lett. **45**, 494 (1980).
[5] F. D. M. Haldane, Model for a Quantum Hall Effect without Landau Levels: Condensed-Matter Realization of the "Parity Anomaly", Phys. Rev. Lett. **61**, 2015 (1988).
[6] C. L. Kane and E. J. Mele, Quantum Spin Hall Effect in Graphene, Phys. Rev. Lett. **95**, 226801 (2005).
[7] B. A. Bernevig, T. L. Hughes, and S.-C. Zhang, Quantum spin Hall effect and topological phase transition in HgTe quantum wells, Science **314**, 1757 (2006).
[8] M. König, S. Wiedmann, C. Brüne, A. Roth, H. Buhmann, L. W. Molenkamp, X.-L. Qi, and S.-C. Zhang, Quantum spin Hall insulator state in HgTe quantum wells, Science **318**, 766 (2007).
[9] R. Karplus and J. M. Luttinger, Hall effect in ferromagnetics, Phys. Rev. **95**, 1154 (1954).
[10] C.-Z. Chang*et al.*, Experimental observation of the quantum anomalous Hall effect in a magnetic topological insulator, Science **340**, 167 (2013).

[11] Z. Wang, Y. Chong, J. D. Joannopoulos, and M. Soljačić, Observation of unidirectional backscattering-immune topological electromagnetic states, Nature **461**, 772 (2009).
[12] G. Jotzu, M. Messer, R. Desbuquois, M. Lebrat, T. Uehlinger, D. Greif, and T. Esslinger, Experimental realization of the topological Haldane model with ultracold fermions, Nature **515**, 237 EP (2014).
[13] Z. Yang, F. Gao, X. Shi, X. Lin, Z. Gao, Y. Chong, and B. Zhang, Topological Acoustics, Phys. Rev. Lett. **114**, 114301 (2015).
[14] S. Klembt, T. H. Harder, O. A. Egorov, K. Winkler, R. Ge, M. A. Bandres, M. Emmerling, L. Worschech, T. C. H. Liew, M. Segev, C. Schneider, and S. Höfling, Exciton-polariton topological insulator, Nature **562**, 552 (2018).
[15] C.-E. Bardyn, T. Karzig, G. Refael, and T. C. H. Liew, Topological polaritons and excitons in garden-variety systems, Phys. Rev. B **91**, 161413 (2015).
[16] A. V. Nalitov, D. D. Solnyshkov, and G. Malpuech, Polariton $\mathbb{Z}$ Topological Insulator, Phys. Rev. Lett. **114**, 116401 (2015).
[17] D. R. Gulevich, D. Yudin, I. V. Iorsh, and I. A. Shelykh, Kagome lattice from an exciton-polariton perspective, Phys. Rev. B **94**, 115437 (2016).
[18] K. Yi and T. Karzig, Topological polaritons from photonic Dirac cones coupled to excitons in a magnetic field, Phys. Rev. B **93**, 104303 (2016).
[19] O. Bleu, D. D. Solnyshkov, and G. Malpuech, Interacting quantum fluid in a polariton Chern insulator, Phys. Rev. B **93**, 085438 (2016).
[20] S. Mandal, R. Ge, and T. C. H. Liew, Antichiral edge states in an exciton polariton strip, Phys. Rev. B **99**, 115423 (2019).
[21] H. Sigurdsson, Y. S. Krivosenko, I. V. Iorsh, I. A. Shelykh, and A. V. Nalitov, Spontaneous topological transitions in polariton condensates due to spin bifurcations, arXiv:1905.12137 (2019).
[22] T. Karzig, C.-E. Bardyn, N. H. Lindner, and G. Refael, Topological Polaritons, Phys. Rev. X **5**, 031001 (2015).
[23] A. Janot, B. Rosenow, and G. Refael, Topological polaritons in a quantum spin Hall cavity, Phys. Rev. B **93**, 161111 (2016).
[24] V. K. Kozin, I. A. Shelykh, A. V. Nalitov, and I. V. Iorsh, Topological metamaterials based on polariton rings, Phys. Rev. B **98**, 125115 (2018).
[25] Y. Otani, B. Pannetier, J. Nozières, and D. Givord, Magnetostatic interactions between magnetic arrays and superconducting thin films, J. Magn. Magn. Mater. **126**, 622 (1993).
[26] P. Vavassori, O. Donzelli, V. Metlushko, M. Grimsditch, B. Ilic, P. Neuzil, and R. Kumar, Magnetic switching in submicron-scale periodic magnetic arrays, J. Appl. Phys. **88**, 999 (2000).
[27] O. Bleu, D. D. Solnyshkov, and G. Malpuech, Photonic versus electronic quantum anomalous Hall effect, Phys. Rev. B **95**, 115415 (2017).
[28] S. Erdin, A. F. Kayali, I. F. Lyuksyutov, and V. L. Pokrovsky, Interaction of mesoscopic magnetic textures with superconductors, Phys. Rev. B **66**, 014414 (2002).
[29] I. F. Lyuksyutov and V. L. Pokrovsky, Ferromagnet-superconductor hybrids, Adv. Phys. **54**, 67 (2005).
[30] A. P. Prudnikov, Yu. A. Bychkov, and O. I. Marichev, *Integrals and Series. Volume 2. Special Functions* (Fizmalit, Moscow, 2003).
[31] C. Schneider, A. Rahimi-Iman, N. Y. Kim, J. Fischer, I. G. Savenko, M. Amthor, M. Lermer, A. Wolf, L. Worschech, V. D. Kulakovskii, I. A. Shelykh, M. Kamp, S. Reitzenstein, A. Forchel, Y. Yamamoto, and S. Höfling, An electrically pumped polariton laser, Nature **497**, 348 EP (2013).
[32] T. Fukui, Y. Hatsugai, and H. Suzuki, Chern numbers in discretized Brillouin zone: Efficient method of computing (spin) Hall conductances, J. Phys. Soc. Jpn. **74**, 1674 (2005).